Measurement of the nonlinear parametric instability gain in dispersion oscillating fibers

Guillaume Vanderhaegen, Pascal Szriftgiser, Alexandre Kudlinski, Andrea Armaroli, Matteo Conforti, Stefano Trillo, Arnaud Mussot

Measurement of the nonlinear parametric instability gain in dispersion oscillating fibers

GUILLAUME VANDERHAEGEN[1,*], PASCAL SZRIFTGISER[1], ALEXANDRE KUDLINSKI[1], ANDREA ARMAROLI[1], MATTEO CONFORTI[1], STEFANO TRILLO[2], AND ARNAUD MUSSOT[1]

[1] University of Lille, CNRS, UMR 8523-PhLAM-Physique des Lasers Atomes et Molécules, F-59000 Lille, France
[2] Department of Engineering, University of Ferrara, 44122 Ferrara, Italy
[*] Corresponding author: guillaume.vanderhaegen@univ-lille.fr

Compiled April 4, 2023

We report the observation of the parametric gain band distortion in the nonlinear (depleted) regime of modulation instability in dispersion oscillating fibers. We show that the maximum gain is shifted even outside the boundaries of the linear parametric gain band. Experimental observations are confirmed by numerical simulations.

http://dx.doi.org/10.1364/ao.XX.XXXXXX

1. INTRODUCTION

Modulation instability (MI) refers to the amplification of a weak perturbation at the expense of a strong pump wave. The first observation in fiber optics had been achieved in 1986 by Tai *et al.* [1] in a conventional telecommunication fiber. The energy transfer from the pump to the perturbation depends on a phase-matching relation in which the nonlinear phase mismatch due to the Kerr effect is balanced by the linear one due to group velocity dispersion. Hence in most experiments, to fulfill this requirement, the pump wave propagates in the anomalous dispersion region of optical fibers. However, there are several other ways to also achieve a perfect compensation of the nonlinear phase mismatch when the dispersion is normal, by exploiting an additional linear contribution of the fiber due to higher-order transverse modes [2], higher-order dispersion terms [3, 4], periodic boundary conditions in resonators [5] or birefringence [6]. A periodic modulation along the propagation direction can also be exploited to trigger the MI process. It was first described in the context of telecom lightwave systems due to their intrinsic periodicity [7, 8], and then observed in fibers suitably engineered with a built-in modulation along the propagation direction [9–12]. In these, so-called dispersion-oscillating fibers (DOFs), the modulation period is a few meters and several sidebands fulfilling a quasi-phase matching relation had been observed over a few THz from the pump. However, in all these experimental investigations (see the review in Ref. [12] for a longer list of works), these new MI sidebands had been investigated in the linear regime of the MI process. In other words, pump depletion has been considered negligible. When this condition breaks down, a general principle [13] tells that one should expect that the sideband frequency for parametric amplification can significantly deviate from the frequency of nonlinear phase-matching that yields the MI gain peak. Depending on the underlying four-photon mixing interaction considered, the optimal frequency has been demonstrated to be lower [14, 15] or higher [16] than the phase-matching frequency. Remarkably, when the MI parametric process is narrowband, the ultimate consequence is that the highest conversion can occur at frequencies outside the linearized gain bandwidth. In other words, it is possible to amplify signals located outside the linear gain band, a phenomenon observed to date in uniform birefringent fibers [14, 16]. Such a striking phenomenon has been also predicted for DOFs by means of mode truncation and averaging techniques [17]. In this letter, we report the observation of this surprising behavior in a DOF. We show that the optimal conversion frequency is blue-shifted up to 11 % from the linearized peak gain frequency, lying clearly outside the bandwidth of the MI gain curve.

2. MODULATION INSTABILITY IN DOFS

We consider a DOF whose group velocity dispersion profile evolves sinusoidally:

$$\beta_2(z) = \beta_{2,\mathrm{avg}} + \beta_{2,\mathrm{amp}} \sin\left(\frac{2\pi}{Z} z\right) \tag{1}$$

where $\beta_{2,\mathrm{avg}}$ is the average GVD value, $\beta_{2,\mathrm{amp}}$ the modulation amplitude around the average value, and Z the oscillation period. Such dispersion profile can easily be obtained by modulating the outer diameter of the fiber during the drawing process [12]. In this work, the relative variation of the outer diameter, and thus of the nonlinear coefficient of the fiber, is about 10%. By working close to the zero dispersion of the fiber, the relative variation of the GVD is close to 30%. We checked numerically that we can neglect the impact of the modulation of the nonlinear coefficient γ compared to the one of the GVD [12, 18]. Thus, we will consider it as constant along the fiber in this work. From the linear stability analysis applied to the nonlinear Schrödinger equation [19] with the GVD evolution described by Eq. (1), one can derive, based on the concept of parametric resonance [18], the frequency offset Ω of the unstable sideband pair that experience peak gain in the m-th order parametric band, for fixed

pump power P_0 [12]:

$$\Omega^2 = \frac{\beta_{2,\mathrm{avg}}}{2}\left[\sqrt{(\gamma P_0)^2 + \left(\frac{m\pi}{Z}\right)^2} - \gamma P_0\right];\ m = 1,2,3\ldots, \quad \textbf{(2)}$$

which can be approximated by the quasi-phase-matching (QPM) relation $\beta_{2,\mathrm{avg}}\Omega^2 + 2\gamma P_0 = \frac{2m\pi}{Z}$, in the limit $\gamma P_0 \ll \frac{m\pi}{Z}$. An infinite number of frequencies are solutions to Eq. (2), but a limited number can indeed be observed because they have to experience a significant gain. Predictions of Eq. (2), combined with a linearized Floquet analysis enable to provide an accurate description of the linear regime of MI in DOFs, revealing the position of the bands and their gain values ([12] and references therein). However, in these works, the power of the perturbation is small compared to the pump power. When propagating in long fibers and/or using strong input signals, this assumption quickly becomes invalid. Under this condition, a simple intuition suggests that strong conversion should be expected at higher frequencies compared with those predicted from Eq. (2) or its QPM approximation. Indeed, when the pump power P_0 decreases because of depletion, the phase-matching frequency predicted by Eq. (2) turns out to increase. Therefore, sidebands which are launched at the right frequency given by Eq. (2) are progressively tuned out of phase-matching as the pump starts to deplete. Conversely, sidebands with initially higher frequency, though initially experience a lower gain, are progressively tuned toward phase-matching, and overall give rise to a better conversion. This heuristic argument is supported by rigorous analysis in [17], which reveals that the linear parametric gain band is strongly distorted shifting towards higher frequencies. For sufficiently strong pump depletion (i.e., sufficiently strong seeding of sidebands at fixed fiber length), the remarkable fact is that the maximum conversion is obtained even outside the parametric gain bandwidth. The analysis shows that, even if the pump is MI-stable in this regime, the strong conversion is supported by an unstable mixed sideband-pump mode which bifurcates from the pump mode [17]. We illustrate this feature by means of the numerics reported in Fig. 1. The dispersion profile along the fiber length is depicted in Fig. 1 (a). The GVD is all normal with an average value $\beta_{2,\mathrm{avg}} = 9.5$ ps^2/km, an amplitude value $\beta_{2,\mathrm{amp}} = 3.1$ ps^2/km and a period of modulation of 200 m. These parameters will be used in our experiments. We display the power evolution of the pump (blue lines) and signal (red lines) along the propagation distance in Fig. 1 (c-d) for a weak (signal to pump power ratio of -50 dB, Fig. 1 (c)) and strong input signal (signal to pump power ratio of -10 dB, Fig. 1 (d)). We calculated the signal power evolution along the fiber length for two characteristics frequency shifts, either in the linear parametric gain band ($f_m = 230$ GHz, see Fig. 1 (b)) or outside ($f_m = 244$ GHz, see Fig. 1 (b)). In all examples depicted in Fig. 1 (c) and (d), the signal experiences periodic modulations equal to the GVD modulation period [12], which is characteristic of DOFs. When the signal power is weak (Fig. 1 (c), 50 dB below the pump power), and located within the parametric gain ($f_m = 230$ GHz), it is amplified during its propagation along the fiber length (solid red line in Fig. 1 (c)). A net gain of 8.2 dB is observed at the fiber output. For a signal located outside the parametric gain band ($f_m = 244$ GHz), the overall gain is negligible (dashed red line in Fig. 1 (c)). The signal experiences a slight growth and decay that is attributed to a standard four-wave mixing process [20], thus to beating without significant energy exchanges between the waves. Predictions from the linear stability analysis are relevant in these cases. Fig. 1 (d) summarizes the nonlinear case when the signal to pump power ratio is increased to -10 dB. When the signal is located within the linear parametric gain band ($f_m = 230$ GHz), it is first amplified and then saturates around 1.2 km before decreasing due to the saturation of the process (solid red line in Fig. 1 (d)). The energy transfers are reversed back as it may happen in the nonlinear regime of MI in uniform fibers. The phenomenon is referred to as Fermi-Pasta-Ulam-Tsingou process [21], and it was also predicted in DOFs [17]. When the signal located outside the parametric gain band ($f_m = 244$ GHz), it keeps growing during its propagation to reach a larger value at the fiber output (dashed red line in Fig. 1 (d)) compared to the signal located within that band. Note that the pump is depleted at the same time, revealing a typical signature of the nonlinear regime of MI [17]. To get a deeper insight, we calculated from numerics the gain curve as a function of the frequency shift and plot them in Fig. 1 (b) for the linear (solid black line) and nonlinear (dashed black line) regimes. In the linear regime, the gain curve is well predicted by the Floquet analysis. The slight discrepancies are due to the finite amplitude of the perturbation and to the relatively small propagation length. In the nonlinear regime, the maximum conversion is shifted outside the parametric gain curve (cuttoff frequency $f_c = 236$ GHz) at $f_m = 245$ GHz. A very similar feature was observed with MI from fiber birefringence in [16].

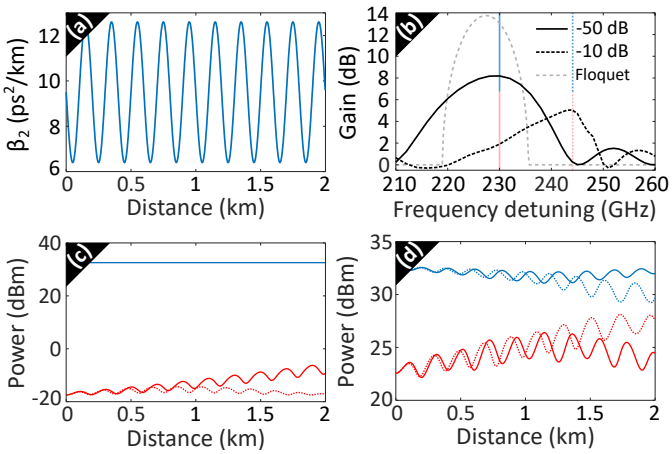

Fig. 1. (a) Longitudinal dispersion profile of the fiber with $\beta_{2,\mathrm{avg}} = 9.5$ ps^2/km, $\beta_{2,\mathrm{amp}} = 3.1$ ps^2/km. (b) Evolution of the fiber output gain as a function of the modulation frequency for an input signal to pump power ratio of -50 dB (solid black line) and -10 dB (dashed black line). The gain band from the Floquet analysis (dashed grey line) is superimposed. (c-d) Evolution of the pump (blue lines) and signal (red lines) power along the fiber length. Solid lines: $f_m = 230$ GHz; dotted lines: $f_m = 244$ GHz. (c) Signal to pump power ratio -50 dB. (d) Signal to pump power ratio -10 dB. Parameters: $\gamma = 4.4$ W^{-1}km^{-1}, $P_p(z=0) = 1.8$ W, $L = 2$ km, $Z = 200$ m.

3. FIBER PARAMETERS AND EXPERIMENTAL SETUP

The $L = 1.72$ km long fiber was fabricated from a Ge-doped preform provided by Exail. The core has a refractive index difference of 17×10^{-3}. The outer diameter was modulated with a sine function of $Z = 200$ m period during the drawing process, resulting in a diameter variation from 113 μm to 123 μm, as shown in Fig. 2 (a), and a core diameter between 3.55 μm and 3.85 μm. At the operating wavelength $\lambda_0 = 1555$ nm, we

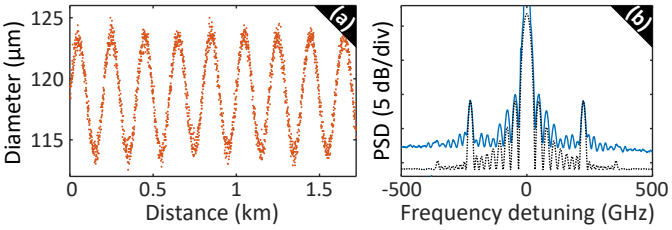

Fig. 2. (a) Measured data of the fiber diameter. (b) Recorded fiber output spontaneous spectra (solid blue line) with the Raman pump switch on. The numerical gain spectrum from numerical simulations [12, 22] is also superimposed (dotted black line).

estimated the fiber attenuation $\alpha = 1.2$ dB/km. The average dispersion has been determined at λ_0 nm to $\beta_{2,\mathrm{avg}} = 9.5\,\mathrm{ps}^2/\mathrm{km}$ and the dispersion amplitude to $\beta_{2,\mathrm{amp}} = 3.1\,\mathrm{ps}^2/\mathrm{km}$, which maximizes the agreement between the measured spontaneous MI spectrum at $P_0 = 1.8$ W (solid blue line in Fig. 2 (b)), with the numerically simulated one using the method of [22] (dotted black line in Fig. 2 (b))). As the average dispersion is pretty large, a single MI sideband is destabilized [12]. Note that we actively compensated the fiber attenuation, to preserve an almost constant pump power in order to get a significant parametric gain value of about 8-9 dB. We implemented a contra-propagating Raman pump as in [23]. With Raman pump power at 1450 nm of $P_R = 600$ mW, the linear attenuation had been reduced to an almost negligible effective value of $\alpha_{\mathrm{eff}}(@1550\ \mathrm{nm}) = 0.25$ dB/km. To study the evolution of the gain curve induced by the nonlinear regime of the MI process, we implemented a setup to measure the on/off gain (difference of the probe gain between the parametric resonance switched on and off) with a pump-probe experiment. It is schematically detailed in Fig. 3. A 1555 nm CW laser, the pump, is shaped into a train of 50 ns

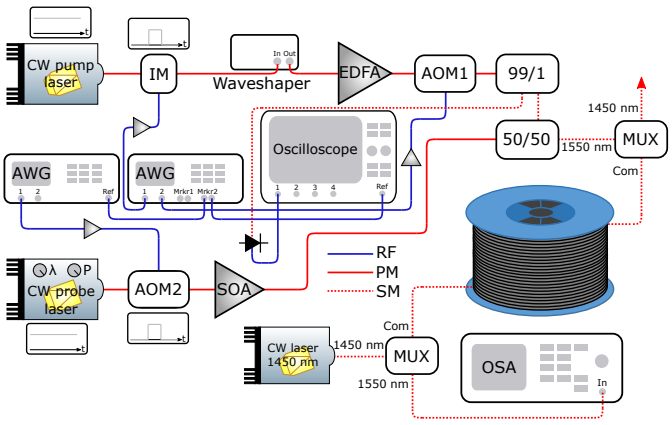

Fig. 3. Sketch of the experimental setup. CW: continuous wave, IM: intensity modulator, AWG: arbitrary waveform generator, AOM: acousto-optic modulator, MUX : multiplexer, SOA: semiconductor amplifier, EDFA: erbium-doped fiber amplifier, OSA: optical spectrum analyser.

pulses through an intensity modulator at a repetition rate of 9.6 kHz, which allows for avoiding stimulated Brillouin scattering (SBS). They are then amplified into an erbium-doped fiber amplifier (EDFA) to reach several Watt peak power. The pulse train passes through an acousto-optic modulator (AOM1) to lower the inter-pulses noise floor, generated by the amplified spontaneous emissions of the EDFA at such low duty cycle (48×10^{-5}). Another CW tunable laser, the probe, is shaped into a similar pulse train by using another acousto-optic (AOM2) modulator and synchronized to the pump. It is also amplified with a semiconductor optical amplifier before being combined with the pump laser through a 50/50 coupler. The pulse train made of a pump and probe signals is then injected inside the DOF. The output spectrum is recorded with an optical spectrum analyzer to measure the on/off gain. Such recordings are automated to get a 2D plot of the on/off gain as a function of the pump-probe frequency shift and of the input signal power. This recording into a $(f_m, P_s(z=0))$ plane provides a detailed illustration of the evolution of the MI process from the linear to the nonlinear regime. It enables to to get a better understanding of the whole dynamics of the process.

4. EXPERIMENTAL RESULTS

The gain experienced by the probe from the parametric resonance is measured over the whole first sidelobe ($m = 1$ in Eq. 1), from 200 to 260 GHz, and for signal to pump power ratios varying from -38 to -10 dB. The on/off gain measurements are summarized in the 2D plot in Fig. 4 (a). To clearly delimit the boundaries of the linear gain bandwidth, we superimposed vertical white dashed lines for which the parametric gain vanishes in Fig. 4 (a) and (c). For very small input signal power (probe to pump ratio up to -25 dB), the gain band remains unchanged and its maximum is located around $f_0 = 227$ GHz. By increasing the signal power (probe to pump ratio above -25 dB), the gain maximum shifts towards larger frequencies and falls beyond the high-frequency boundary of the linear MI band (dashed white lines) above the power ratio of -17 dB. To get a clearer insight into the modification of the gain shapes, we plot the gain curves for specific values of signal to pump power ratio, for -35 dB (blue line), -14.9 dB (orange line) and -10 dB (yellow line), in Fig. 4 (b). This clearly reveals a 25.8 GHz (11%) shift from the maximum of the linear gain curve for a power ratio of -10 dB. The progressive evolution of the maximum gain frequency (blue crosses), and the corresponding gain (red crosses) as a function of the input signal to pump power ratios are illustrated in Fig. 4 (e). It highlights the decrease of the gain value at the same time as the frequency shift increases which was not easy to observe in the 2D plot. Finally, the progressive evolution towards the nonlinear stage of the parametric process is also noticeable referring to the maximum conversion efficiency curve, as it was done in Ref. [14] (Fig. 4 (f)). Indeed, even if the gain is lower for large signals condition, what really matters is the conversion efficiency, which accounts for the sidebands (signal and idler) power fraction after the parametric amplification process. We observe a linear increase of the conversion efficiency (measured at the maximum gain) with respect to the probe to pump ratio (note the horizontal log scale) up to the value of -20 dB, above which the curve tends to saturate. The latter can be explained by the saturation of the parametric gain. All these experimental results are confirmed by numerical results obtained by integrating the NLSE (Fig. 4 (c-f)).

5. CONCLUSION

We have reported the first observation of the nonlinear stage of the parametric instability occurring in DOFs. This was achieved with a pump-probe experiment, through a fine-tuning of the probe amplitude and frequency shift from the pump. It revealed

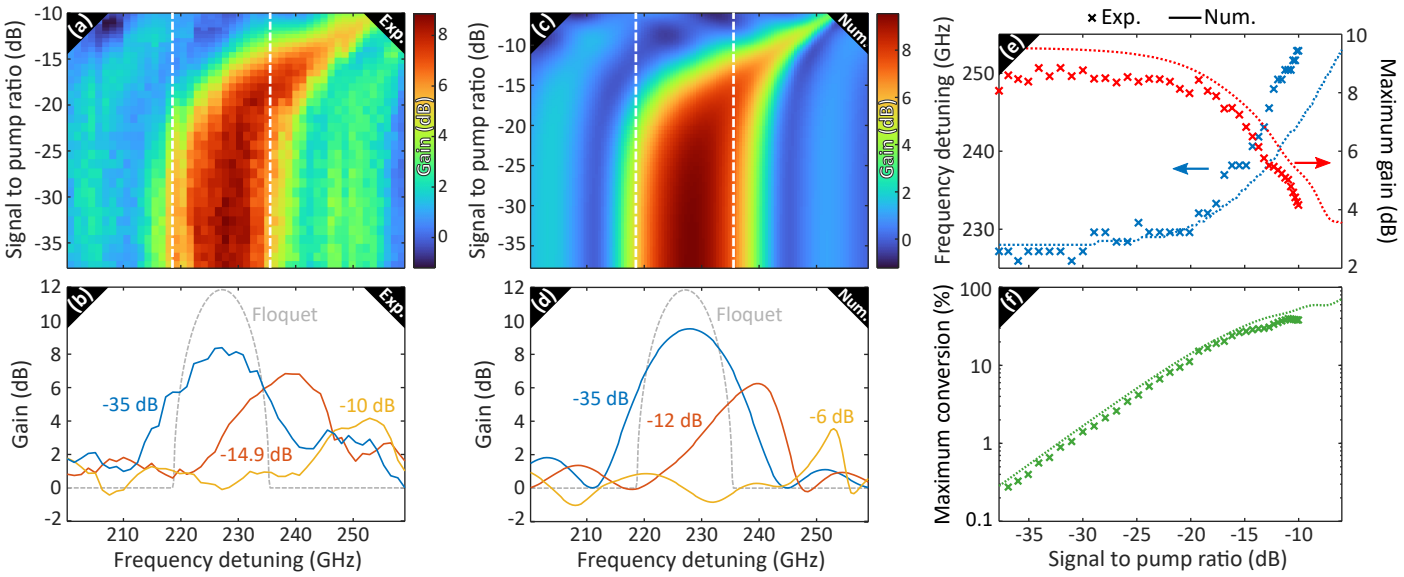

Fig. 4. (a)-(c) Evolution of the gain experienced by the probe from the parametric process as a function of the pump-probe frequency detuning and the power ratio. The vertical dashed white lines account for the cutoff frequencies of the gain band predicted by the Floquet analysis. (b)-(d) Evolutions of the gain for specific values of signal to pump power ratios. The dashed grey line accounts for the gain band predicted by the Floquet analysis. (a-b): experimental data. (c-d): data from NLSE numerical integration. (e-f): evolutions of (e) the maximum gain frequency (blue) and the maximum gain value (red), and (f) the maximum conversion efficiency as a function of the signal to pump power ratio. Crosses: experimental data. Dotted lines: numerical data.

the transition from a linear regime of instability to a nonlinear regime. The latter exhibits a completely distorted parametric gain curve, with a maximum value shifted outside the limit of the parametric gain (of about 26 GHz, equivalent to $\sim$ 11 % from the peak of the gain curve) together with a decrease of the maximum gain value. These experimental results had been confirmed by numerics. Another interesting aspect, which will be the subject of a future work, is to study the periodic conversion from the pump to the sidebands, which was predicted in Ref. [17]. This is similar to the better-known phenomenon of Fermi-Pasta-Ulam-Tsingou recurrences, observed in uniforms optical fibers [21, 23]. Given the large out-of-band gain discovered here, this will allow us to better understand the dynamics of nonlinear MI in non-integrable dynamical systems.

Funding. This work was supported by the Agence Nationale de la Recherche (Programme Investissements d'Avenir FARCO project, I-SITE VERIFICO); Ministry of Higher Education and Research; Hauts de France Council (GPEG project); European Regional Development Fund (Photonics for Society P4S) and the CNRS (IRP LAFONI) and H2020 Marie Skłodowska-Curie Actions (MSCA)(713694) and MEFISTA and University of Lille Through the LAI HOLISTIC. We acknowledge Exail for the fabrication of the preform. S.T. acknowledges Ministero dell'Università e della Ricerca (2020X4T57A).

Disclosures. The authors declare no conflicts of interest.

Data availability. Data underlying the results presented in this paper are not publicly available at this time but may be obtained from the authors upon reasonable request.

REFERENCES

1. K. Tai, A. Hasegawa, and A. Tomita, Phys. Rev. Lett. **56**, 135–138 (1986).
2. R. Stolen, IEEE J. Quantum Electron. **11**, 100 (1975).
3. A. Y. H. Chen, G. K. L. Wong, S. G. Murdoch, R. Leonhardt, J. D. Harvey, J. C. Knight, W. J. Wadsworth, and P. S. J. Russell, Opt. Lett. **30**, 762 (2005).
4. S. Pitois and G. Millot, Opt. Commun. **226**, 415 (2003).
5. S. Coen and M. Haelterman, Phys. Rev. Lett. **79**, 4139 (1997).
6. S. Wabnitz, Phys. Rev. A **38**, 2018–2021 (1988).
7. F. Matera, A. Mecozzi, M. Romagnoli, and M. Settembre, Opt. Lett. **18**, 1499 (1993).
8. N. J. Smith and N. J. Doran, Opt. Lett. **21**, 570 (1996).
9. M. Droques, A. Kudlinski, G. Bouwmans, G. Martinelli, and A. Mussot, Opt. Lett. **37**, 4832 (2012).
10. M. Droques, A. Kudlinski, G. Bouwmans, G. Martinelli, and A. Mussot, Phys. Rev. A **87**, 013813 (2013).
11. C. Finot, J. Fatome, A. Sysoliatin, A. Kosolapov, and S. Wabnitz, Opt. Lett. **38**, 5361 (2013).
12. A. Mussot, M. Conforti, S. Trillo, F. Copie, and A. Kudlinski, Adv. Opt. Photonics **10**, 1 (2018).
13. S. Trillo, G. Millot, E. Seve, and S. Wabnitz, Appl. Phys. Lett. **72**, 150 (1998).
14. G. Millot, E. Seve, S. Wabnitz, and S. Trillo, Phys. Rev. Lett. **80**, 504–507 (1998).
15. A. Bendahmane, A. Mussot, A. Kudlinski, P. Szriftgiser, M. Conforti, S. Wabnitz, and S. Trillo, Opt. Express **23**, 30861 (2015).
16. E. Seve, G. Millot, and S. Trillo, Phys. Rev. E **61**, 3139 (2000).
17. M. Conforti, A. Mussot, A. Kudlinski, S. Rota Nodari, G. Dujardin, S. De Biévre, A. Armaroli, and S. Trillo, Phys. Rev. Lett. **117**, 013901 (2016).
18. A. Armaroli and F. Biancalana, Opt. Express **20**, 25096–25110 (2012).
19. G. Agrawal, *Nonlinear Fiber Optics* (Academic Press, 2012).
20. G. Vanderhaegen, C. Naveau, P. Szriftgiser, A. Kudlinski, M. Conforti, A. Mussot, M. Onorato, S. Trillo, A. Chabchoub, and N. Akhmediev, Proc. National Acad. Sci. **118**, e2019348118 (2021).
21. G. Van Simaeys, P. Emplit, and M. Haelterman, Phys. Rev. Lett. **87**, 033902 (2001).
22. M. Marhic, F. Yang, M.-C. Ho, and L. Kazovsky, J. Light. Technol. **17**, 210–215 (1999).
23. C. Naveau, G. Vanderhaegen, P. Szriftgiser, G. Martinelli, M. Droques, A. Kudlinski, M. Conforti, S. Trillo, N. Akhmediev, and A. Mussot, Front. Phys. **9**, 25 (2021).

FULL REFERENCES

1. K. Tai, A. Hasegawa, and A. Tomita, "Observation of modulational instability in optical fibers," Phys. Rev. Lett. **56**, 135–138 (1986).
2. R. Stolen, "Phase-matched-stimulated four-photon mixing in silica-fiber waveguides," IEEE J. Quantum Electron. **11**, 100– 103 (1975).
3. A. Y. H. Chen, G. K. L. Wong, S. G. Murdoch, R. Leonhardt, J. D. Harvey, J. C. Knight, W. J. Wadsworth, and P. S. J. Russell, "Widely tunable optical parametric generation in a photonic crystal fiber," Opt. Lett. **30**, 762–764 (2005).
4. S. Pitois and G. Millot, "Experimental observation of a new modulational instability spectral window induced by fourth-order dispersion in a normally dispersive single-mode optical fiber," Opt. Commun. **226**, 415–422 (2003).
5. S. Coen and M. Haelterman, "Modulational Instability Induced by Cavity Boundary Conditions in a Normally Dispersive Optical Fiber," Phys. Rev. Lett. **79**, 4139–4142 (1997).
6. S. Wabnitz, "Modulational polarization instability of light in a nonlinear birefringent dispersive medium," Phys. Rev. A **38**, 2018–2021 (1988).
7. F. Matera, A. Mecozzi, M. Romagnoli, and M. Settembre, "Sideband instability induced by periodic power variation in long-distance fiber links," Opt. Lett. **18**, 1499 (1993).
8. N. J. Smith and N. J. Doran, "Modulational instabilities in fibers with periodic dispersion management," Opt. Lett. **21**, 570 (1996).
9. M. Droques, A. Kudlinski, G. Bouwmans, G. Martinelli, and A. Mussot, "Experimental demonstration of modulation instability in an optical fiber with a periodic dispersion landscape," Opt. Lett. **37**, 4832 (2012).
10. M. Droques, A. Kudlinski, G. Bouwmans, G. Martinelli, and A. Mussot, "Dynamics of the modulation instability spectrum in optical fibers with oscillating dispersion," Phys. Rev. A **87**, 013813 (2013).
11. C. Finot, J. Fatome, A. Sysoliatin, A. Kosolapov, and S. Wabnitz, "Competing four-wave mixing processes in dispersion oscillating telecom fiber," Opt. Lett. **38**, 5361 (2013).
12. A. Mussot, M. Conforti, S. Trillo, F. Copie, and A. Kudlinski, "Modulation instability in dispersion oscillating fibers," Adv. Opt. Photonics **10**, 1 (2018).
13. S. Trillo, G. Millot, E. Seve, and S. Wabnitz, "Failure of phase-matching concept in large-signal parametric frequency conversion," Appl. Phys. Lett. **72**, 150–152 (1998).
14. G. Millot, E. Seve, S. Wabnitz, and S. Trillo, "Observation of a novel large-signal four-photon instability in optical wave mixing," Phys. Rev. Lett. **80**, 504–507 (1998).
15. A. Bendahmane, A. Mussot, A. Kudlinski, P. Szriftgiser, M. Conforti, S. Wabnitz, and S. Trillo, "Optimal frequency conversion in the nonlinear stage of modulation instability," Opt. Express **23**, 30861–30871 (2015).
16. E. Seve, G. Millot, and S. Trillo, "Strong four-photon conversion regime of cross-phase-modulation-induced modulational instability," Phys. Rev. E **61**, 3139–3150 (2000).
17. M. Conforti, A. Mussot, A. Kudlinski, S. Rota Nodari, G. Dujardin, S. De Biévre, A. Armaroli, and S. Trillo, "Heteroclinic structure of parametric resonance in the nonlinear Schrödinger equation," Phys. Rev. Lett. **117**, 013901 (2016).
18. A. Armaroli and F. Biancalana, "Tunable modulational instability sidebands via parametric resonance in periodically tapered optical fibers," Opt. Express **20**, 25096–25110 (2012).
19. G. Agrawal, *Nonlinear Fiber Optics* (Academic Press, 2012).
20. G. Vanderhaegen, C. Naveau, P. Szriftgiser, A. Kudlinski, M. Conforti, A. Mussot, M. Onorato, S. Trillo, A. Chabchoub, and N. Akhmediev, ""Extraordinary" modulation instability in optics and hydrodynamics," Proc. National Acad. Sci. **118**, e2019348118 (2021).
21. G. Van Simaeys, P. Emplit, and M. Haelterman, "Experimental Demonstration of the Fermi-Pasta-Ulam Recurrence in a Modulationally Unstable Optical Wave," Phys. Rev. Lett. **87**, 033902 (2001).
22. M. Marhic, F. Yang, M.-C. Ho, and L. Kazovsky, "High-nonlinearity fiber optical parametric amplifier with periodic dispersion compensation," J. Light. Technol. **17**, 210–215 (1999).
23. C. Naveau, G. Vanderhaegen, P. Szriftgiser, G. Martinelli, M. Droques, A. Kudlinski, M. Conforti, S. Trillo, N. Akhmediev, and A. Mussot, "Heterodyne Optical Time Domain Reflectometer Combined With Active Loss Compensation: A Practical Tool for Investigating Fermi Pasta Ulam Recurrence Process and Breathers Dynamics in Optical Fibers," Front. Phys. **9**, 25 (2021).